THE JOURNAL OF BIOLOGICAL CHEMISTRY VOL. 291, NO. 49, pp. 25427–25438, December 2, 2016

The Stalk Domain of NKp30 Contributes to Ligand Binding and Signaling of a Preassembled NKp30-CD3ζ Complex*[S]

Received for publication, June 10, 2016, and in revised form, September 21, 2016 Published, JBC Papers in Press, October 17, 2016, DOI 10.1074/jbc.M116.742981

Stefanie Memmer[‡§1], Sandra Weil[‡§1], Steffen Beyer[§], Tobias Zöller[¶], Eike Peters[§‖], Jessica Hartmann[**], Alexander Steinle[¶], and Joachim Koch[‡§‡‡2]

From the [‡]Institute of Medical Microbiology and Hygiene, University of Mainz Medical Center, 55131 Mainz, Germany, the [§]Institute for Tumor Biology and Experimental Therapy, Georg-Speyer-Haus, 60596 Frankfurt am Main, Germany, the [¶]Institute for Molecular Medicine, Goethe-University Frankfurt am Main, 60528 Frankfurt am Main, Germany, the [‖]Institute for Microbiology, ETH Zürich, 8093 Zürich, Switzerland, the [**]Division of Molecular Biotechnology and Gene Therapy, Paul-Ehrlich-Institut, 63225 Langen, Germany, and the [‡‡]LOEWE Excellence Center for Cell and Gene Therapy, 60590 Frankfurt am Main, Germany

Edited by Peter Cresswell

The natural cytotoxicity receptor (NCR) NKp30 (CD337) is a key player for NK cell immunosurveillance of infections and cancer. The molecular details of ligand recognition and its connection to CD3ζ signaling remain unsolved. Here, we show that the stalk domain ([129]KEHPQLGAGTVLLLR[143]) of NKp30 is very sensitive to sequence alterations, as mutations lead to impaired ligand binding and/or signaling capacity. Surprisingly, the stalk domains of NKp30 and NKp46, another NCR employing CD3ζ for signaling, were not exchangeable without drastic deficiencies in folding, plasma membrane targeting, and/or ligand-induced receptor signaling. Further mutational studies, *N*-glycosylation mapping, and plasma membrane targeting studies in the absence and presence of CD3ζ suggest two interconvertible types of NCR-CD3ζ assemblies: 1) a signaling incompetent structural NKp30-CD3ζ complex and 2) a ligand-induced signaling competent NKp30-CD3ζ complex. Moreover, we propose that ligand binding triggers translocation of Arg-143 from the membrane interface into the membrane to enable alignment with oppositely charged aspartate residues within CD3ζ and activation of CD3ζ-signaling.

Natural killer (NK)[3] cells belong to the family of innate lymphoid cells and are of outstanding importance for immune surveillance of infections and cancer (1–5). Unlike cytotoxic T lymphocytes, NK cells kill without prior sensitization via the polarized release of cytotoxic granules containing perforin and granzymes (6, 7). NK cells are activated by target cells with low or absent expression of MHC class I ("missing-self") and/or stress-induced expression of ligands for activating NK cell receptors ("induced-self") (3). Consequently, the activation state of NK cells is governed by a predominance of signals from germ line-encoded inhibitory or activating surface receptors. Major activating receptors are NKG2D (also known as KLRK1 and CD314) (8) and the immunoglobulin-like NCRs, NKp30 (also known as NCR3, NCTR3, and CD337) (9), NKp44 (also known as NCR2, NCTR2, and CD336) (10, 11), and NKp46 (also known as NCR1, NCTR1, and CD335) (12, 13). A large number of pathogen-associated ligands have been identified for the NCRs. However, the number of known cellular ligands and knowledge about their mode of action is still scarce (2). NKp30 recognizes the tumor antigens B7-H6 (14) and BCL-2-associated athanogene 6 (BAG-6, also known as BAT3) (15, 16). Recently galectin-3, which is released by many types of tumor cells, was proposed as an inhibitory ligand for NKp30 (17). For NKp44, the nuclear protein proliferating cell nuclear antigen (PCNA) (18) and an isoform of the mixed lineage leukemia-5 (MLL-5) protein (19) were identified as ligands. So far, no cellular ligands have been identified for NKp46. All NCRs are type I membrane proteins composed of an ectodomain with one (NKp30 and NKp44) or two (NKp46) immunoglobulin (Ig)-like domains connected to a membrane-spanning α-helix via a stalk domain, and a short cytosolic tail. For signaling, the NCRs associate with immunoreceptor tyrosine-based activating motif (ITAM)-bearing adaptor molecules, such as CD3ζ/FcεRIγ (NKp30 and NKp46) or DAP12 (NKp44) (2). The functional importance of this interaction is illustrated by the finding that NK cells from knock-out mice lacking CD3ζ and FcεRIγ showed reduced cytolytic activity toward a large number of tumor cell lines (20). Moreover, previous studies showed a reduced number of T cell receptor (TCR) molecules on the surface of T cells due to intracellular retention of TCRs in the absence of CD3ζ (21–23). The NMR structure of a disulfide-stabilized transmembrane helix dimer of CD3ζ has been solved (PDB code 2HAC; Ref. 24) demonstrating proximity of two

* This work was supported by grants from the Deutsche Forschungsgemeinschaft (KO 4368/3-1), the LOEWE Center for Cell and Gene Therapy Frankfurt supported by Hessisches Ministerium für Wissenschaft und Kunst (HMWK) funding reference number III L 4-518/17.004 (2010), the Alfons und Gertrud Kassel-Stiftung, the Research Support Foundation (Vaduz, Switzerland), and the Uniscientia Stiftung (Vaduz, Switzerland). The authors declare that they have no conflicts of interest with the contents of this article.

[S] This article contains supplemental Table S1 and Figs. S1–S7.

[1] Both authors contributed equally to this work.

[2] To whom the correspondence should be addressed: Immunobiology of Natural Killer Cells, Institute of Medical Microbiology and Hygiene, University of Mainz Medical Center, Obere Zahlbacher Str. 67, D-55131 Mainz, Germany. Tel.: 49-6131-17-9336; Fax: 49-6131-17-9234; Email: joachim.koch@uni-mainz.de.

[3] The abbreviations used are: NK, natural killer; NCR, natural cytotoxicity receptor; BAG-6, BCL-2-associated athanogene 6; Ig, immunoglobulin; ITAM, immunoreceptor tyrosine-based activating motif; DAP12, DNAX activation protein of 12 kDa; TCR, T cell receptor; TM, transmembrane; OST, oligosaccharyl transferase; ER, endoplasmic reticulum; ANOVA, analysis of variance.

aspartate residues to the outer membrane leaflet. These two aspartate residues are believed to form an intramembrane charge contact with positively charged residues in the transmembrane (TM) region of the TCR α chain, NKp30, and NKp46 (2, 25).

Recently, we have shown that the stalk domain of NKp30 increases the affinity for binding of its cognate ligands B7-H6 and BAG-6 (26, 27) presumably involving stalk-dependent clustering of NKp30 (28). In the current study we have investigated the contribution of individual amino acids within the stalk domain of NKp30 to ligand binding and formation of a signaling-competent NKp30-CD3ζ complex. Based on these studies, we propose a mechanistic model of how ligand binding to the ectodomain of NKp30 is communicated across the plasma membrane via CD3ζ to enable cellular signaling.

Results

The Stalk Domains of NKp30 and NKp46 Are Functionally Non-equivalent—In a previous study we showed that the stalk domain of NKp30 contributes to ligand binding and represents a functional domain of NKp30 (27, 28). Even though NKp30 and NKp46 differ in the number of Ig domains and the sequence and length of their stalk domains, they both signal via CD3ζ (2) (supplemental Fig. S1). Based on these data, we first asked whether the ectodomains of NKp30 and NKp46 represent individual functional entities. Therefore, we generated NKp30/NKp46 chimera with exchanged Ig domains or exchanged stalk domains (Fig. 1*A*). These chimera or their wild type counterparts were stably expressed in A5-GFP-signaling reporter cells, which constitutively express CD3ζ and allow for quantification of ligand induced signaling based on proportional GFP expression (supplemental Fig. S2). First, we investigated expression and plasma membrane targeting of the NCR chimera by flow cytometry. All of the NCR constructs were expressed; however, besides the wild type (WT) NCRs, only chimera containing the Ig domain of NKp30 and the stalk of NKp46 (NKp30Ig/46Stalk/46TM and NKp30Ig/46Stalk/30TM) were targeted to the plasma membrane (Fig. 1, *B* and *C*). These data suggest that although the stalk domain of NKp46 is compatible with NKp30 maturation, the stalk domain of NKp30 is unable to maintain folding, plasma membrane targeting, and retention of NKp46. Next, we investigated the signaling capacity of the different receptor mutants. Therefore, A5-GFP cells transduced with NCR variants were stimulated with plate-bound NKp30- or NKp46-specific antibodies and subsequently analyzed for GFP expression by flow cytometry. Strikingly, both chimera containing the Ig domain of NKp30 (NKp30Ig/46Stalk/46TM and NKp30Ig/46Stalk/30TM) showed receptor signaling comparable with NKp30 WT (Fig. 1*D*). These data show principal functionality of these chimera with respect to signaling via CD3ζ. As expected, no signaling was observed for NKp46Ig/30Stalk/30TM and NKp46Ig/30Stalk/46TM, which were not present on the cell surface (Fig. 1*E*). Next, we asked whether the NCR chimera containing the Ig domain of NKp30 display ligand-induced signaling. Therefore, NCR-transduced A5-GFP cells were co-cultured with Ba/F3 B7-H6 cells according to previously published procedures (26, 27). Surprisingly, the NKp30 ligand B7-H6 was unable to induce CD3ζ signaling and related GFP expression of the two chimera containing the Ig domain of NKp30 (NKp30Ig/46Stalk/46TM and NKp30Ig/46Stalk/30TM) (Fig. 1*F*). These data demonstrate that the Ig domain and the stalk domain of NKp30 and presumably of NKp46 are a functional unit that mediates ligand-induced conformational changes required for CD3ζ signaling. Moreover, these data suggest that the stalk domain of NKp30 contains specific sequence motifs required for its function.

Functionality of NKp30 Is Impaired by Alterations in the Amino Acid Sequence of the Stalk Domain—To investigate the individual contribution of specific amino acids within the stalk domain of NKp30 to ligand binding and ligand-induced signaling, we performed systematic alanine scanning mutagenesis in the context of NKp30::hIgG1-Fc (NKp30-Fc) fusion proteins (27).

Therefore, binding of 14 alanine mutants of NKp30-Fc fusion proteins to immobilized biotinylated B7-H6-Fc fusion proteins was analyzed by surface plasmon resonance and kinetic parameters (K_a and K_d) as well as equilibrium dissociation constants (K_D) were determined (Table 1 and supplemental Fig. S3). As both, NKp30 and B7-H6 were present as Fc fusion proteins, data were fitted with the bivalent analyte model. In this model one analyte molecule (A) can bind to one or two ligand molecules (B), and both analyte binding sites are assumed to be equivalent.

$$A + B \underset{K_{d1}}{\overset{K_{a1}}{\rightleftharpoons}} AB \qquad \text{(Eq. 1)}$$

$$AB + B \underset{K_{d2}}{\overset{K_{a2}}{\rightleftharpoons}} AB_2 \qquad \text{(Eq. 2)}$$

where K_{a1} is the association rate constant for the formation of AB, K_{a2} is the association rate constant for formation of AB_2, K_{d1} is the dissociation rate constant for complex AB, and K_{d2} is the dissociation rate constant for complex AB_2.

K_D values were determined from the initial NKp30/B7-H6 interaction, as binding to the second site does not change the refractive index and, therefore, does not give rise to a response.

$$K_D = \frac{K_{d1}}{K_{a1}} \qquad \text{(Eq. 3)}$$

According to χ^2 values, bivalent analyte fit was sufficient for all sensograms (Table 1). A K_D value of 84 nM was obtained for NKp30 WT, which was in accordance with previous measurements (27). Comparison of the alanine mutants showed that mutation of the amino acids close to the Ig fold had the most dramatic effect, leading to K_D values in the micromolar range. The greater the distance between the alanine mutation and the Ig fold, the less prominent was the effect on K_D values. Alanine mutations of the membrane-proximal amino acids showed K_D values similar to NKp30 WT except for the Arg-143 alanine mutant (R143A), which displayed a slightly higher K_D value.

Additionally, equilibrium dissociation constants (K_D) of the 14 alanine mutants were determined by ELISA with a fragment of the NKp30 ligand BAG-6 (BAG-$6_{686-936}$) according to pre-

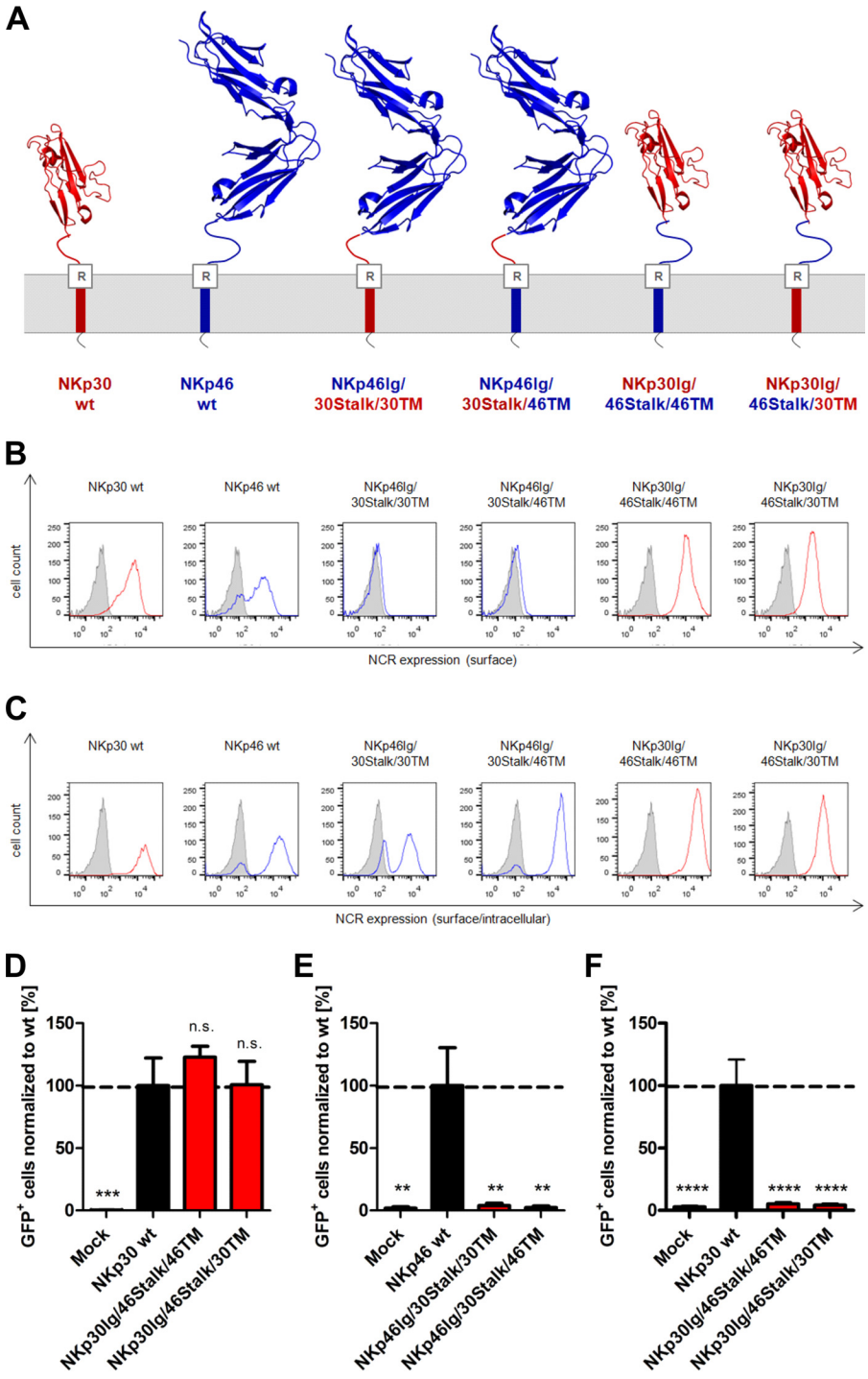

FIGURE 1. **Expression and receptor signaling of NKp30/NKp46 chimera.** *A*, schematic representation of NKp30 WT (*red*, PDB code 3NOI), NKp46 WT (*blue*, PDB code 1P6F), and NKp30/NKp46 chimera (NKp30 domains in *red*, NKp46 domains in *blue*) in the plasma membrane. *B* and *C*, surface (*B*) and intracellular (*C*) expression of the receptors and the corresponding NKp30/NKp46 chimera in transduced A5-GFP cells analyzed by flow cytometry. *Gray*, mock control; *red*, anti-NKp30; *blue*, anti-NKp46. One representative experiment of three is shown. *D–F*, signaling reporter assays of transduced A5-GFP cells after stimulation with plate-bound NKp30-specific (*D*) or NKp46-specific antibodies (*E*) and after co-incubation with Ba/F3 B7-H6 cells (*F*). GFP expression was analyzed by flow cytometry of $CD4^+$/$SytoxBlue^-$ A5-GFP cells. The percentage of GFP-positive cells normalized to NKp30 WT is indicated as the mean ± S.E. of three independent experiments measured in duplicate. Statistical significance of flow cytometry experiments was assessed by one-way ANOVA and Dunnett's multiple comparisons test with Prism 6 software. *n.s.*, not significant ($p > 0.05$); **, $p = 0.001–0.01$; ***, $p = 0.0001–0.001$; ****, $p < 0.0001$.

viously published procedures (26, 27). Interestingly, most of the alanine substitutions were tolerated without loss of binding affinity to BAG-$6_{686-936}$ as indicated by similar K_D values of the mutated and wild type NKp30-Fc fusion proteins (supplemental Table S1). However, substitution of the first (K129A) or either one of the last three amino acids (L141A, L142A, R143A) of the stalk domain led to lower binding affinity to BAG-$6_{686-936}$ as indicated by increased K_D values (supplemental Table S1).

Because all of the receptor fusion proteins were expressed in a human cell line and purified from culture supernatant after

TABLE 1

Kinetic parameters and equilibrium dissociation constants for binding of NKp30 variants to B7-H6 as determined by SPR

RU, response units.

NKp30 variant	K_{a1}	K_{d1}	K_D	K_{a2}	K_{d2}	R_{max}	χ^2
	1/ms	*1/s*		*1/RUs*	*1/s*	*RU*	
WT	1.848×10^5	0.01568	84.8 nM	1.695×10^{-4}	4.747×10^{-4}	29.51	0.0450
K129A	3.983×10^3	0.01024	2.6 μM	1.010×10^{-4}	3.565×10^{-4}	82.87	0.200
E130A	1.067×10^4	0.02601	2.4 μM	2.819×10^{-4}	1.754×10^{-4}	151.4	0.266
H131A	4.317×10^3	0.007382	1.7 μM	1.251×10^{-4}	2.043×10^{-4}	92.42	0.141
P132A	2.239×10^5	0.01715	76.6 nM	2.038×10^{-4}	7.947×10^{-4}	79.02	0.819
Q133A	2.672×10^3	0.02109	7.9 μM	2.927×10^{-4}	2.683×10^{-4}	36.05	0.0672
L134A	1.854×10^5	0.02435	131.3 nM	2.622×10^{-4}	6.582×10^{-4}	82.98	1.5
G135A	7.102×10^3	0.005343	752.3 nM	3.222×10^{-4}	2.295×10^{-4}	178.6	0.0825
G137A	8.123×10^4	0.005512	67.9 nM	0.002121	0.004202	71.58	3.16
T138A	9.709×10^3	0.006610	680.8 nM	4.297×10^{-4}	4.354×10^{-4}	13.13	0.274
V139A	4.008×10^5	0.01453	36.3 nM	1.432×10^{-4}	0.001044	68.01	0.414
L140A	4.527×10^5	0.01768	39.1 nM	2.254×10^{-4}	0.001179	19.99	0.0296
L141A	1.930×10^5	0.01538	79.7 nM	1.855×10^{-4}	5.017×10^{-4}	25.05	0.0224
L142A	3.830×10^5	0.01705	44.5 nM	1.894×10^{-4}	5.507×10^{-4}	23.29	0.0466
R143A	3.622×10^4	0.009299	253.9 nM	2.068×10^{-4}	3.115×10^{-4}	46.95	0.0075

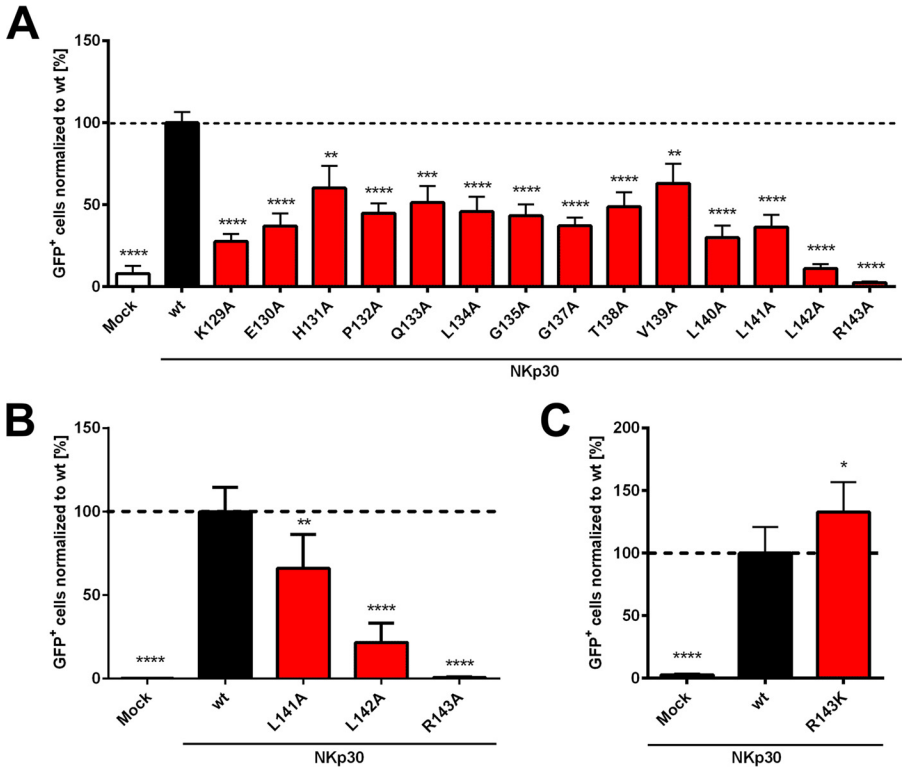

FIGURE 2. **Contribution of individual amino acids of the NKp30 stalk to signaling.** *A–C*, A5-GFP cells transduced with the different NKp30 alanine mutants or a lysine mutant of Arg-143 were analyzed for their signaling capacity after co-incubation with Ba/F3 B7-H6 cells (*A* and *C*) or after stimulation with plate-bound NKp30-specific antibodies (*B*). GFP expression was analyzed by flow cytometry of $CD4^+$/$SytoxBlue^-$ A5-GFP cells. The percentage of GFP-positive cells normalized to wild type is indicated as the mean ± S.E. of three independent experiments measured in duplicate. Statistical significance of flow cytometry experiments was assessed by one-way ANOVA and Dunnett's multiple comparisons test with Prism 6 software. *, $p = 0.01–0.05$; **, $p = 0.001–0.01$; ***, $p = 0.0001–0.001$; ****, $p < 0.0001$.

secretion, they have passed cellular quality control. Moreover, the constructs show preserved B_{max} values in the ELISA setting, demonstrating equivalent numbers of binding receptive molecules in the different samples. Therefore, the differences in K_D values can be attributed to differences in ligand binding affinity for cognate ligand.

To investigate whether ligand binding of the individual NKp30 mutants is correlated with their capacity to promote ligand-induced CD3ζ signaling, we performed A5-GFP signaling reporter assays by stimulation with Ba/F3 B7-H6 cells. Signaling capacity of NKp30 was reduced by alanine mutation at any of the amino acids within the stalk domain. Most drastic loss of function was seen for the two amino acids at the transition of the N-terminal Ig-domain and the stalk domain of NKp30 (K129A and E130A) and the three C-terminal leucine residues at the transition of the stalk domain to the transmembrane domain (L140A, L141A, and L142A) (Fig. 2*A*). As expected, mutation of Arg-143, which is believed to mediate an intramembrane charge contact with CD3ζ, led to a complete loss of signaling capacity (Fig. 2*A*). Notably, signaling reporter assays were performed at saturating conditions for >12 h, therefore excluding that slight differences in expression levels

of the NKp30 variants (supplemental Fig. S4) might affect determination of their signaling capacity. To evaluate whether the loss of signaling capacity of the mutants was due to a failure of NKp30 to mediate ligand-induced conformational changes or to a lack of specific motifs generally needed for communication with CD3ζ, we performed signaling reporter assays after receptor stimulation with plate-bound NKp30-specific antibodies. Interestingly, the L141A and L142A mutants showed reduced signaling capacity, demonstrating that both residues with particular emphasis on Leu-142 are important for CD3ζ signaling (Fig. 2*B*). As expected, again the NKp30 variant devoid of Arg-143 (R143A) showed no CD3ζ signaling. Notably, Leu-140, Leu-141, Leu-142, and Arg-143 are highly conserved among species (supplemental Fig. S5). These data demonstrate that several steps might be needed to communicate ligand binding of the ectodomain of NKp30 to CD3ζ. To investigate whether ligand-induced NKp30 signaling requires the side chain of Arg-143 or only a positively charged residue at position 143, we performed signaling reporter assays with a lysine variant of NKp30 (R143K) after stimulation with Ba/F3 B7-H6 cells. Surprisingly, the signaling capacity of the R143K mutant was maintained or even improved when compared with NKp30 WT, demonstrating that a positive charge at position 143 is essential and sufficient for NKp30 function (Fig. 2*C*).

Transmembrane Residues Other Than Arg-143 Are Dispensable for NKp30 Signaling—Based on our results, we hypothesized that ligand binding initiates a stalk-dependent shift of the transmembrane domain of NKp30 to push Arg-143 more deeply into the membrane for association with CD3ζ and presumably to expose residues from the lipid interface to secondary effector molecules in the cytoplasm. Therefore, we investigated the contribution of conserved amino acids (Ala-144, Gly-145, Tyr-161, Tyr-162, and Tyr-165) in the proximity of Arg-143 and the transition of the transmembrane domain and the cytosolic domain of NKp30 (Fig. 3). First, we tested whether the tyrosine residues (Tyr-161 and Tyr-162) close to the transition of the transmembrane domain and the cytosolic domain of NKp30 contribute to CD3ζ signaling (Fig. 3*A*). The single mutants Y161F and Y162F and the double mutant Y161F/Y162F were expressed equally well in transduced A5-GFP cells (Fig. 3*B*). However, mutation of these residues did not alter receptor signaling after stimulation with Ba/F3 B7-H6 target cells (Fig. 3*C*), suggesting no specific requirement of Tyr-161 and Tyr-162 for CD3ζ signaling.

Relocation of Arg-143 within the membrane during CD3ζ signaling might require strong forces to overcome charge repellence of the hydrophobic membrane interface. This might be achieved by ligand-induced oligomerization (28, 29) and an unpolar "lid" generated by Leu-140, Leu-141, and Leu-142 preceding Arg-143. This hypothesis is supported by the finding that these leucine residues were intolerant to alanine substitution without loss of NKp30 signaling capacity (Fig. 2, *A* and *B*). Therefore, we tested whether leucine substitution of the two amino acids succeeding Arg-143 and, thus, reduction of charge repellence of Arg-143, could render NKp30 signaling independent of ligand binding (Fig. 3). Even though the double mutant A144L/G145L was expressed equally well as NKp30 WT (Fig. 3*B*), it showed no increase in signaling capacity (Fig. 3*D*) and no GFP expression (signaling) without ligand stimulation (Fig. 3*E*). In the next step we tried to uncouple receptor signaling from ligand binding by systematically shifting Arg-143 toward the C terminus of NKp30 while otherwise preserving the sequence order of NKp30. We expected that in one of these constructs the arginine residue would permanently align with a cognate aspartate residue of CD3ζ. Surprisingly, none of the constructs was expressed on the cell surface, demonstrating that a positive charge might not be tolerated permanently within the inner core of NKp30's transmembrane domain. Finally, prediction of the location of the transmembrane domain of NKp30 based on TMpred (30) implies that the transmembrane domain is anchored between two flanking positive charges (Arg-143 and Tyr-165). Therefore, we tried to uncouple CD3ζ signaling from ligand binding to NKp30 by combined mutation of Ala-144 and Gly-145 and the shift of Tyr-165 to amino acid position 161 (A144L/G145L/Lys-165→161) to force Arg-143 into the inner core of the membrane for contact with CD3ζ (Fig. 3*A*). Even though expression of the A144L/G145L/Lys-165→161 construct was preserved (Fig. 3*B*), we observed only moderate reduction of signaling capacity in A5-GFP signaling reporter assays (Fig. 3*D*) and no GFP expression (signaling) without ligand stimulation (Fig. 3*E*).

Altogether, these data argue for a strong charge-repellence, which keeps the side chain of Arg-143 at the transition interface between extracellular region and membrane. Alignment of Arg-143 with the aspartate of CD3ζ in order to enable signaling might be achieved by ligand-induced receptor clustering and stalk-dependent conformational changes.

Arg-143 of NKp30 Is Positioned Directly at the Membrane Interface—To analyze the positioning of Arg-143 in the ground state, we performed *N*-glycosylation scanning mutagenesis. *N*-glycosylation of eukaryotic membrane proteins is catalyzed by a membrane-associated oligosaccharyl transferase (OST) complex in the lumen of the endoplasmic reticulum (ER). The OST complex transfers an oligosaccharide to the side chain of an asparagine (Asn) acceptor in the N*X*(S/T) motif (where *X* can be every amino acid except proline). According to the 12 + 14 rule, such an acceptor site must be placed a minimum of 14 amino acids N-terminal or 12 amino acids C-terminal from the membrane surface to be *N*-glycosylated because the active site of the OST complex is positioned a certain distance away from the ER membrane (31). This minimal distance can be used to map the ends of TM segments of membrane proteins (29, 32, 33). Therefore, *N*-glycosylation acceptor sites are introduced 14 amino acids N-terminal from the amino acid to be analyzed. The addition of an oligosaccharide adds about 2 kDa to the protein and is visible as motility shift in SDS-PAGE. Although the presence of glycosylation indicates that the amino acid to be analyzed is located outside of the membrane, the absence of glycosylation is not that conclusive, as it might be due to the fact that the used N*X*(S/T) motif is an inefficient acceptor site or is located too close to the membrane (34).

Within the current study, we performed *N*-glycosylation mutagenesis to analyze the positioning of key amino acids of NKp30 (Leu-140, Arg-143, Tyr-147) and NKp46 (Asn-255, Arg-258, Ala-262) that were assumed to be near the membrane transition interface. Therefore, an OST acceptor site was intro-

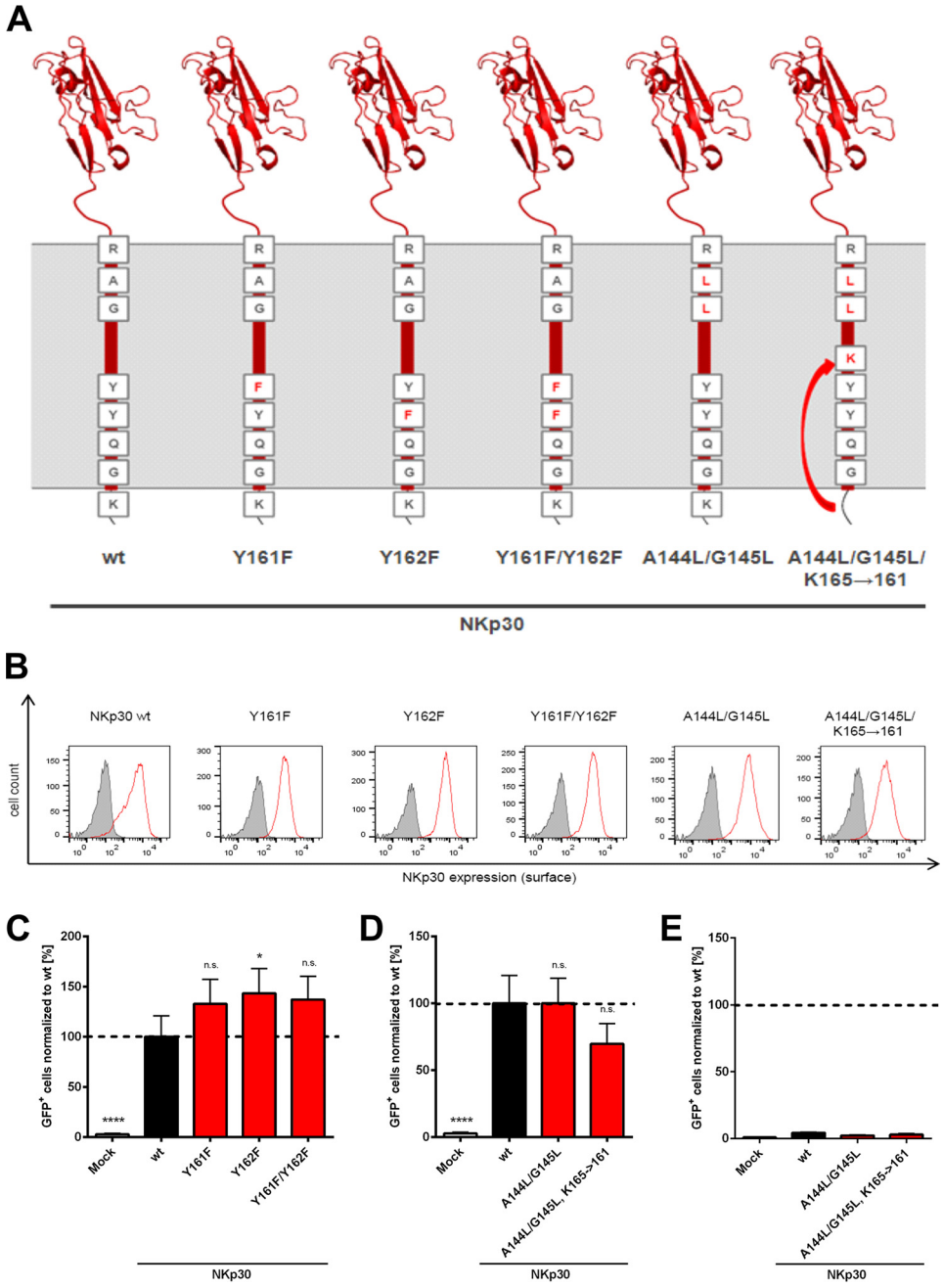

FIGURE 3. **Influence of specific amino acids within or in the vicinity of the transmembrane domain of NKp30 on CD3ζ signaling.** *A*, schematic representation of NKp30 WT (PDB code 3NOI) and NKp30 mutants in the plasma membrane. Natural amino acids are shown in *black*, and mutated amino acids are shown in *red*. *B*, surface expression of the receptor mutants in A5-GFP cells analyzed by flow cytometry. *Gray*, isotype control; *red*, anti-NKp30. One representative experiment of three is shown. *C* and *D*, signaling of transduced A5-GFP cells after co-incubation with Ba/F3 B7-H6 cells in comparison to A5-GFP cells transduced with NKp30 WT and A5-GFP cells transduced with the empty transfer vector (*Mock*). GFP expression was analyzed by flow cytometry of $CD4^+$/SytoxBlue$^-$ A5-GFP cells. The percentage of GFP-positive cells normalized to wild type is indicated as the mean ± S.E. of three independent experiments measured in duplicate. Statistical significance of flow cytometry experiments was assessed by one-way ANOVA and Dunnett's multiple comparisons test with Prism 6 software. *E*, signaling of transduced A5-GFP cells after co-incubation with Ba/F3 Mock cells in comparison to A5-GFP cells transduced with NKp30 WT and A5-GFP cells transduced with the empty transfer vector (*Mock*). GFP expression was analyzed by flow cytometry of $CD4^+$/SytoxBlue$^-$ A5-GFP cells and normalized to the percentage of GFP-positive NKp30 wild type cells after co-incubation with Ba/F3 B7-H6 cells (compare with Fig. 4*D*). *n.s.*, not significant ($p > 0.05$); *, $p = 0.01–0.05$; ****, $p < 0.0001$.

duced 14 positions N-terminal from each residue to be analyzed (Fig. 4*A*). 293T/17 cells were transduced with the NKp30 and NKp46 constructs. All mutants were detectable on the plasma membrane of the cells, indicating that the introduced *N*-glycosylation sites did not affect membrane targeting (Fig. 4, *B* and *C*). Thereby, artifacts caused by glycosylation of constructs that were not inserted correctly into the membrane could be excluded. Western blotting analysis of the NKp30 constructs compared with NKp30 WT revealed that only the V126N/E128S mutant is additionally glycosylated, speaking for the fact that Leu-140 of NKp30 is positioned outside of the membrane, whereas Arg-143 seems to be located directly at the transition interface in ground state (indicated by absent glycosylation of K129N/H131S and Q133N/G135S; Fig. 4*D*). In contrast to that,

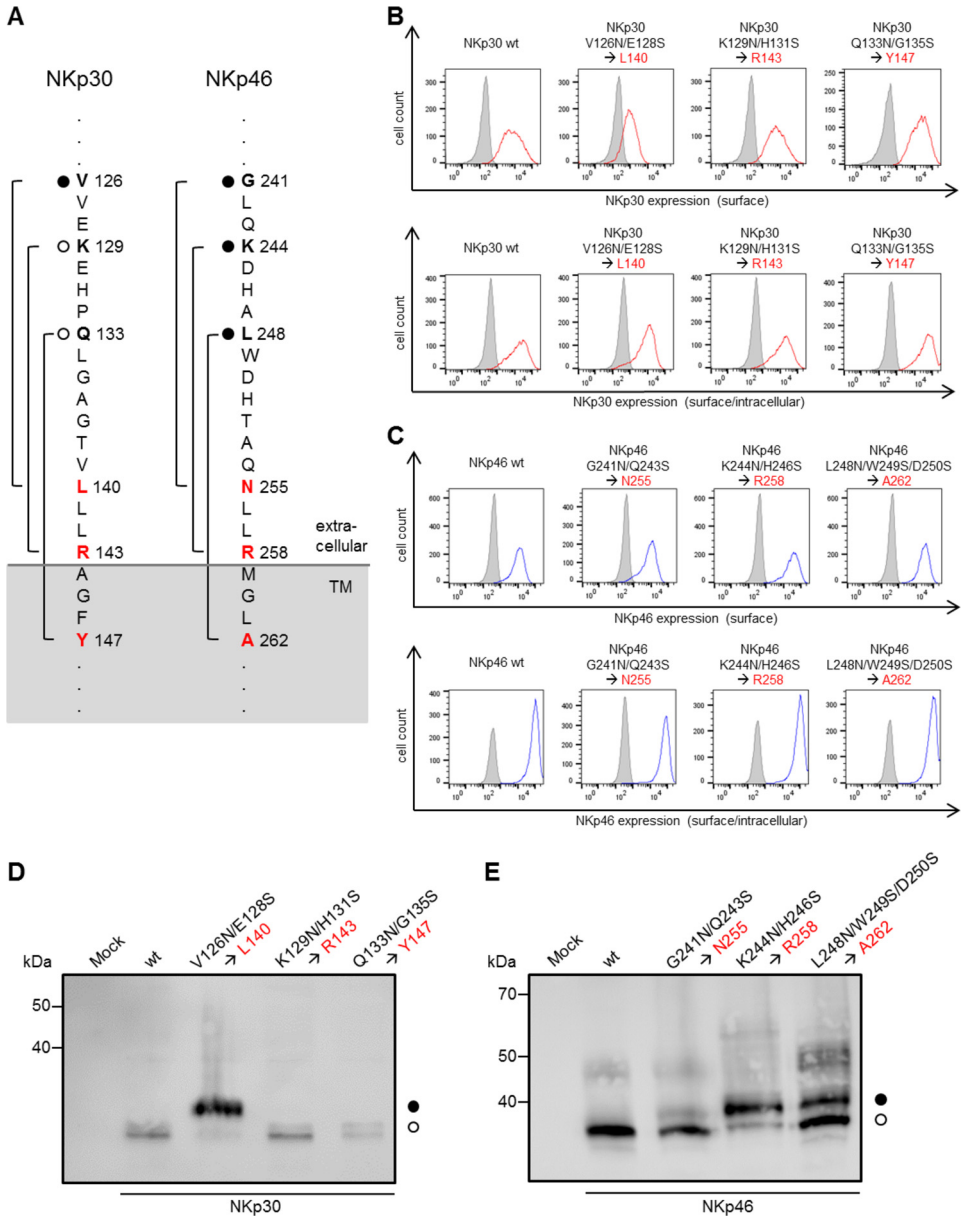

FIGURE 4. **Positioning of amino acids at the membrane transition interface.** *A*, schematic representation of the *N*-glycosylation scanning. Amino acids mutated to *N*-glycosylation acceptor sites are shown in *bold*, and amino acids to be analyzed at the membrane transition interface are shown in *red*. *Brackets* indicate the 14 amino acids between *N*-glycosylation sites and the amino acids to be analyzed. *Solid circles*, glycosylated sites after mutation; *open circles*, non-glycosylated sites after mutation. *B* and *C*, plasma membrane and intracellular expression of the NKp30 (*B*) and NKp46 (*C*) mutants in transduced 293T/17 cells analyzed by flow cytometry. *D* and *E*, Western blotting analysis of NKp30 (*D*) and NKp46 (*E*) mutants detected with NKp30- or NKp46-specific antibodies, respectively. One representative experiment of three is shown.

glycosylation of all three corresponding mutants was detectable in case of NKp46, showing not only that Arg-258 is located outside of the membrane but also that it is located at least 4 amino acids away from the transition interface in the extracellular region (Fig. 4*E*).

NKp30 and NKp46 Form Structural Complexes with CD3ζ in the Absence of Ligand—Our results suggest that the stalk domain is critical to communicate ligand binding at the ectodomain of NKp30 to CD3ζ. However, at this stage it was unclear whether these events are essential to activate a pre-existing NKp30-CD3ζ complex or whether they enable recruitment of CD3ζ to a preactivated receptor-ligand complex. Therefore, we investigated the interaction of NKp30 and NKp46 with CD3ζ in non-lymphoid cells. HeLa cells stably expressing CD3ζ were additionally transduced with the different receptor variants. Expression of NKp30, NKp46, and CD3ζ was confirmed by confocal laser scanning microscopy after detection with specific antibodies (Fig. 5*A*). Interestingly, NKp30 and NKp46 co-localized with CD3ζ at the plasma membrane in the absence of ligand. Additionally, confocal laser scanning microscopy analysis of the NKp30 alanine mutants showed co-localization of all the different receptor variants including L140A, L141A, L142A, and R143A with CD3ζ (supplemental Fig. S6). This indicates that the membrane-proximal amino acids are involved in signal transduction at the NKp30-CD3ζ interface rather than in assembly of the NKp30-CD3ζ complex. Moreover, compara-

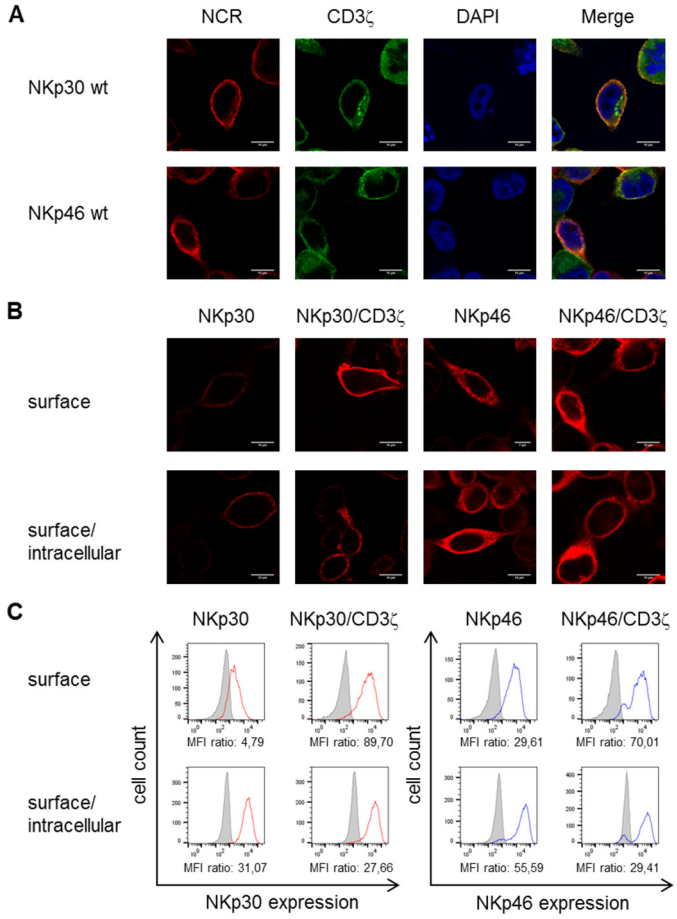

FIGURE 5. **Folding, plasma membrane targeting, and retention of NKp30 and NKp46 depend on CD3ζ.** *A*, immunofluorescence staining of CD3ζ-transduced HeLa cells additionally transduced with either NKp30 or NKp46. *Red*, surface staining of the NCRs with specific antibodies; *green*, intracellular staining of CD3ζ with specific antibodies; *blue*, DAPI; *size bar*, 10 μm. One representative picture of at least five is shown. *B*, immunofluorescence microscopy analysis of NKp30 and NKp46 expression (plasma membrane and intracellular) in HeLa cells with or without CD3ζ. *Red*, staining of the NCRs with specific antibodies; *size bar*, 10 μm. One representative picture of at least five is shown. *C*, flow cytometric analysis of NKp30 and NKp46 expression (plasma membrane and intracellular) in HeLa cells with or without CD3ζ. *Gray*, isotype control; *red*, anti-NKp30; *blue*, anti-NKp46. Median fluorescence intensity (*MFI*) ratios (MFI of NCR staining normalized to MFI of isotype control staining) are indicated. One representative experiment of three is shown.

tive immunofluorescence and flow cytometric studies of HeLa cells expressing NKp30 or NKp46 alone and in combination with CD3ζ showed higher NCR expression levels in the presence of CD3ζ, indicating that both NKp30 and NKp46 require CD3ζ for efficient plasma membrane targeting and/or retention (Fig. 5, *B* and *C*). Taken together, these results demonstrate formation of structural NKp30-CD3ζ and NKp46-CD3ζ complexes without the requirement of auxiliary factors specific for lymphoid cells and without requiring a pre-activated receptor ligand complex. Therefore, ligand-induced conformational changes of NKp30 and NKp46 might enable activation of preformed NKp30-CD3ζ and NKp46-CD3ζ complexes, respectively.

Discussion

NK cells recognize and eliminate malignantly transformed cells after ligation of major activating receptors to their cognate antigens on the plasma membrane of tumor cells (2). Only few cellular ligands of the NCRs have been identified so far; among these are BAG-6 and B7-H6. Molecularly, little is known about ligand binding and its communication to the corresponding signaling adaptor proteins such as the ITAM-containing proteins CD3ζ (NKp30 and NKp46) or DAP12 (NKp44). Notably, CD3ζ also acts as a signaling adaptor for TCR signaling (14, 16, 35). Previously, we showed that the stalk domain of NKp30 (^{129}KEHPQLGAGTVLLLR^{143}) impacts ligand binding and CD3ζ signaling (27). Based on these data the current study focused on the contribution of individual amino acids within the stalk domain of NKp30 to ligand binding and formation of a signaling-competent NKp30-CD3ζ complex. Based on NKp30/NKp46 chimera, we found that the ectodomains of NKp30 and NKp46 form functional entities of an Ig domain and a cognate stalk domain, as the NKp30 stalk domain was incompatible with folding and plasma membrane targeting of NKp46 and the stalk domain of NKp46 was incompatible with ligand-induced signaling of NKp30 (Fig. 1). Intracellular retention of the chimera containing the Ig domains of NKp46 and the stalk domain of NKp30 might be explained by the length differences of the two stalk domains. As the stalk domain of NKp30 is much shorter than the stalk domain of NKp46, this might lead to steric hindrance of the membrane incorporation of the chimera. Notably, even though the stalk domain of NKp30 was indispensable as a transition interface for communication of ligand binding, the stalk domain of NKp46 was sufficient to maintain principal signaling capacity of NKp30, as demonstrated by retained signaling of the NKp30Ig/46Stalk/46TM and NKp30Ig/46Stalk/30TM chimera after antibody cross-linking (Fig. 1). This phenotype might be partially explained by preservation of a sequence motif of the NKp30 stalk in the membrane-proximal sequence stretch of NKp46 ($^{129/244}$K(-)HLLR$^{143/258}$; (-) indicates a negatively charged amino acid; supplemental Fig. S1), which seems to confer principal signaling capacity independent of the stalk length. Notably, His-131 in the NKp30 stalk is not conserved among species (supplemental Fig. S5).

Another possibility to explain the phenotype of the NKp30/NKp46 chimera is a reduced binding affinity for B7-H6 when compared with NKp30 WT, which in turn might lead to insufficient cross-linking of the mutants. However, cell decoration experiments with soluble B7-H6::hIgG1-Fc fusion proteins showed a correlation of NKp30 expression and B7-H6 binding, indicating that signaling of the mutants is not influenced by impaired ligand binding (supplemental Fig. S7).

Alanine scanning mutagenesis showed that the stalk domain of NKp30 is sensitive to alterations in amino acid sequence as demonstrated by substantial loss of B7-H6 binding and signaling capacity (Fig. 2 and Table 1). Interestingly, differential alterations in ligand binding affinity (direct receptor-ligand interaction) and avidity (local increase of ligand binding sites due to receptor oligomerization) of the NKp30 stalk mutants were found for the two cellular ligands BAG-6 and B7-H6, although the crystal structures of NKp30 (PDB code 3NOI) and NKp30 ligated to B7-H6 (PDB code 3PV6) imply ligand binding at the Ig domain of NKp30 (36, 37). This might be explained by differences in methodology and binding sites of B7-H6 and BAG-6

within NKp30 (26). Interestingly, CD3ζ signaling was maintained when Arg-143, which is believed to enable an intramembrane charge interaction with aspartate residues within CD3ζ (24), was mutated to lysine. However, signaling was lost when Arg-143 was mutated to alanine. In addition to Arg-143, the two preceding leucine residues, which are conserved in NKp30 and NKp46, are of particular importance for NKp30 signaling, suggesting a similar mechanism for signal transition to CD3ζ for both NCRs. Moreover, the presence of several leucine residues in front of the aspartic acid in the transmembrane domain of CD3ζ (24) further indicates the importance of such residues for the signaling interface and presumably for compensating charge repellence of the charged amino acids within the hydrophobic membrane environment. In this context it was surprising to see that insertion of additional leucine residues in the vicinity of Arg-143 to increase local hydrophobicity had no effect on NKp30's signaling capacity (Fig. 3). Moreover, displacement of Arg-143 toward the C terminus of NKp30, in order to bury it more deeply in the membrane and to uncouple ligand binding and CD3ζ signaling, was incompatible with folding and plasma membrane targeting of NKp30. This suggests that Arg-143 might require additional conformational changes of NKp30 to enable translocation of the charged side chain into the membrane or that membrane localization of the charge might only be transiently tolerated. Taken together, these data indicate that efficient ligand binding and its communication to CD3ζ requires a highly defined stalk domain with respect to sequence, conformational properties, and charge.

N-glycosylation mapping showed that Arg-143 of NKp30 is located in close proximity to the interface between membrane and extracellular region, as shown by the fact that Leu-140 is located outside and Arg-143 inside of the membrane (Fig. 4). This location suggests that in ground state Arg-143 is not aligned with the aspartate of CD3ζ, which is located six amino acids farther in the membrane (24). Interestingly, for NKp46, the location of Arg-258 was mapped to be at least four amino acids away from the transmembrane region. This speaks for slightly different conformational changes that are needed for NKp30 and NKp46 activation and could also be another explanation for the fact that the stalk domain of NKp46 is not able to mediate ligand-induced signaling of NKp30.

For T cells it is suggested that both TCR aggregation and conformational changes may play a role for signaling (for review, see Ref. 38). Therefore, it could be assumed that in the case of NKp30, a translocation of Arg-143 from the interface between the membrane and extracellular region into the membrane could either facilitate the association of the receptor-CD3ζ complex or lead to its activation. The fact that the CD3ζ chain clearly increased the plasma membrane expression of NKp30 and NKp46 even in the absence of a ligand, as shown in immunofluorescence and flow cytometry experiments, argues for a preexisting structural NKp30-CD3ζ complex in the plasma membrane of inactive cells. Therefore, Arg-143 more likely provides a switch to induce CD3ζ signaling than promotes assembly of the NKp30-CD3ζ complex. This idea is compatible with previous reports on the TCR-CD3 complex demonstrating that CD3ζ is loosely associated with the TCR in ground state (39) and that CD3ζ is essential for plasma membrane expression of the TCR (22, 40). Previous studies showed that in the presence of lipid, the cytoplasmic tail of CD3ζ is folded, thereby preventing ITAM phosphorylation, whereas in aqueous solution it loses its conformation and can be phosphorylated. This leads to the assumption that without activation, the CD3ζ tail is associated with the plasma membrane and is, therefore, inaccessible to phosphorylation. During activation through receptor cross-linking, it could be released, leading to phosphorylation of the ITAM motifs (41). Additionally, a piston-like movement of the TCR complex upon ligand binding was proposed that could be mediated by the transmembrane domain of CD3εγ (35).

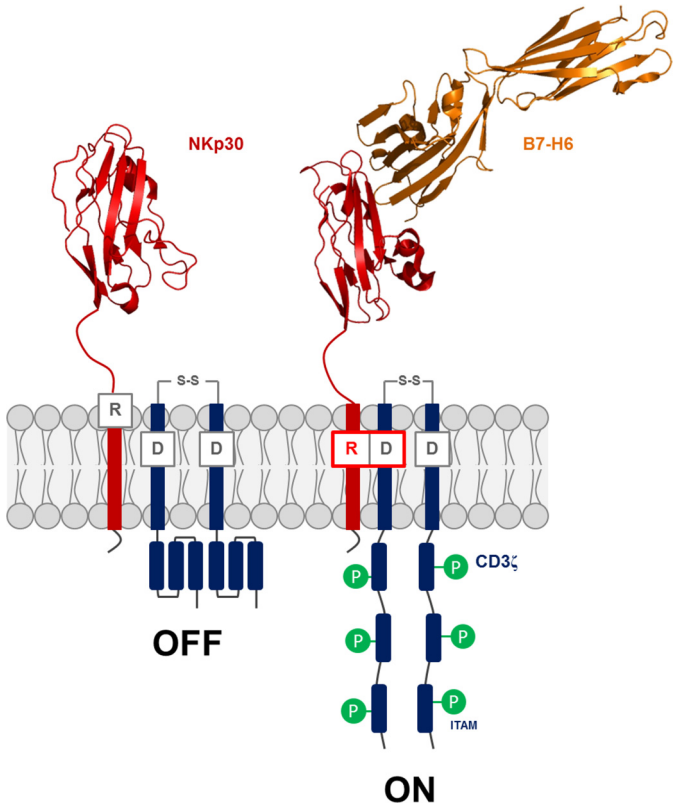

FIGURE 6. **Model for ligand-induced activation of NKp30 and signal transduction to CD3ζ.** In the ground-state (*OFF*), NKp30 (PDB code 3NOI) and CD3ζ form a signaling incompetent structural complex (NKp30-CD3ζ) with Arg-143 placed directly at the plasma membrane interface. Upon ligand binding (NKp30/B7-H6, PDB code 3PV6), conformational changes within NKp30 enable translocation of Arg-143 more deeply into the plasma membrane for alignment with aspartate residues of CD3ζ. Consequently, the structural NKp30-CD3ζ complex is converted into a signaling competent complex (*ON*), which mediates CD3ζ-dependent cellular signaling.

Based on these data we propose two interconvertible types of NCR/CD3ζ assemblies: 1) a signaling-incompetent structural NKp30-CD3ζ complex and 2) a ligand-induced signaling-competent NKp30-CD3ζ complex. Moreover, we suggest that ligand binding to the ectodomain of NKp30 (and presumably NKp46) triggers translocation of Arg-143 (Arg-258 in NKp46) more deeply into the membrane for alignment with the aspartate of CD3ζ and activation of CD3 ζ-signaling (Fig. 6).

Experimental Procedures

Antibodies—The following antibodies were used for flow cytometry and immunofluorescence microscopy: mouse anti-

human NKp30 (P30-15, hybridoma cells kindly provided by C. Watzl), mouse anti-human NKp30 (APC-conjugate, P30-15, BioLegend), mouse anti-human NKp46 (APC-conjugate, 9E2, BioLegend), mouse anti-human NKp46 (n1D9, Abcam), rat anti-mouse CD4 (APC-conjugate, GK1.5, eBioscience), goat anti-human IgG-Fc (Alexa Fluor 647-conjugate, Dianova), and mouse anti-human CD3ζ (FITC-conjugate, 6B10.2, BioLegend). For Western blotting and ELISA, goat anti-human IgG-Fc (HRP conjugate, Sigma), goat anti-human NKp30 (AF1849, R&D Systems), and mouse anti-human NKp46 (195314, R&D) were used. For signaling reporter assays, mouse anti-human NKp30 (210845, R&D Systems) and mouse anti-human NKp46 (195314, R&D Systems) antibodies were used.

Cells—Human cervical carcinoma (HeLa, CCL-2) and human embryonic kidney cell lines (293T/17, CRL-11268) were purchased from the American Type Culture Collection (ATCC). IL-3-independent subclones of the murine pro-B-cell line Ba/F3, transduced with B7-H6 (Ba/F3 B7-H6) or an empty vector (Ba/F3 mock), were kindly provided by C. Watzl, and murine $CD4^+$ T cell hybridoma signaling reporter cells (A5-GFP) were kindly provided by A. Diefenbach (27). *Trichoplusia ni* High Five cells were purchased from Life Technologies. Ba/F3 cells, A5-GFP cells, and High Five cells were cultured as published previously (26, 27); HeLa cells and 293T/17 cells were cultured according to recommendations of ATCC.

Production and Purification of Recombinant Proteins—NKp30 variants (NM_147130.2; residues 19–143) were generated by *de novo* gene synthesis (Genscript), cloned into the pFUSE-hIgG1-FcEQ vector, and expressed in 293T/17 cells as described previously (27). Biotinylated B7-H6::hIgG1-Fc protein was expressed in 293T/17 cells after transfection with pFUSE-B7-H6-hIgG1-FcEQ-Avi vector containing an additional C-terminal Avi tag and plasmids encoding soluble BirA ligase or BirA ligase containing an ER retention sequence. For biotinylation, 20 μM biotin were added to the culture medium during protein production. After 2 days of culture, Fc fusion proteins were purified on protein A-Sepharose as described previously (27). Soluble BAG-$6_{686-936}$ protein was purified from cell culture supernatant of High Five insect cells as described previously (26).

Generation of Lentiviral Vector Particles—Lentiviral particles encoding receptor variants were generated based on codon-optimized cDNA (Genscript) of human NKp30 (NM_147130.2) and human NKp46 (NM_001145457.2). NKp30/NKp46 chimera were generated by exchange of gene segments encoding the extracellular Ig-like domains (NM_147130.2, residues 1–128; NM_001145457.2, residues 1–211) or the stalk domains (NM_147130.2, residues 129–143; NM_001145457.2, residues 212–258) of NKp30 and NKp46, respectively. All constructs containing a C-terminal decahistidine tag were generated by *de novo* gene synthesis (Genscript). The genes of wild type and mutant receptor constructs were cloned into the LeGO-iZ vector (27). For production of lentiviral particles encoding human CD3ζ, the cDNA sequence of CD3ζ (NM_000734.2) was cloned into the LeGO-PuroR vector. Lentiviral particles were produced after PEI transfection of 293T/17 cells with a three-plasmid system (transfer: LeGO-iZ receptor constructs or LeGO-PuroR-CD3ζ; packaging: pCMV-dR8.91; envelope: pMD2.G). Virus-containing supernatant was collected 2–3 days after transfection and concentrated either by low speed centrifugation (2,000 × *g*, 24 h, 4 °C) or ultracentrifugation (100,000 × *g*, 3 h, 4 °C). The virus pellet was resuspended by gentle agitation in 1 ml of fresh culture medium (overnight, 4 °C).

Generation of Stable A5-GFP, 293T/17, and HeLa Cell Lines—A5-GFP and 293T/17 cells were transduced with lentiviral particles encoding receptor variants or lentiviral particles containing the empty LeGo-iZ vector as control. A5-GFP cells were sorted for high surface expression of the receptor mutants and kept in culture with occasional resorting until further use. 293T/17 cells were selected with 150 μg/ml Zeocin. HeLa cells were transduced with lentiviral particles encoding human CD3ζ and selected with puromycin for 2 weeks. CD3ζ expression was verified by flow cytometry after intracellular staining with CD3ζ-specific antibodies. For co-localization experiments, non-transduced or CD3ζ-transduced HeLa cells were additionally transduced with lentiviral particles encoding the different receptor variants.

Flow Cytometry—Surface staining of cells was done with specific antibodies or recombinant human IgG1-Fc fusion proteins diluted in PBS supplemented with 2% FBS. For intracellular staining, the cells were fixed with 4% paraformaldehyde/PBS and afterward permeabilized and stained with specific antibodies or hIgG1-Fc fusion proteins in PBS supplemented with 0.2% saponin, 2% FBS, and 1% BSA. Cells were analyzed on a FAC separation has to be behind FACS, not in between SCantoII instrument with FACSDiva software (BD Biosciences). For cell sorting, cells were stained at sterile conditions with specific antibodies and sorted on a FACSAria instrument with FACS-Diva software (BD Biosciences).

Immunofluorescence Microscopy—Adherent cells were cultured on polylysine-coated glass slides for 16 h, fixed with 4% paraformaldehyde/PBS, and blocked with 5% BSA. For surface staining, cells were incubated with specific antibodies in PBS containing 5% BSA for 1 h. For intracellular staining, cells were permeabilized with 0.2% saponin in 5% BSA/PBS and afterward incubated with specific antibodies for 1 h at room temperature. Subsequently, cells were stained with DAPI and covered with mounting medium. Brightfield and fluorescence images were obtained with a TCS-SP5 laser scanning microscope (Leica) using a HCX PL APO Lbd.Bl 63×/1.4–0.6 oil objective. Images were analyzed using LAS-AF lite 2.0 and ImageJ software.

ELISA—96-Well ELISA plates were coated with 10 μg/ml BAG-$6_{686-936}$ (26) in PBS, blocked with 5% BSA/PBS, and incubated with graded amounts of hIgG1-Fc fusion proteins. Bound hIgG1-Fc fusion proteins were detected with goat anti-human IgG-Fc HRP-conjugated antibodies. Quantification was done in a microtiter plate reader (λ = 450 nm) after conversion of 3,3′,5,5′-tetramethylbenzidine substrate. K_D and B_{max} values were determined by nonlinear regression using Prism 6 software (GraphPad).

Surface Plasmon Resonance—To measure the interaction of the different NKp30::hIgG1-Fc (NKp30-Fc) mutants with the cellular ligand B7-H6, the Biotin CAPture kit (GE Healthcare) and the Biacore T200 system (GE Healthcare) were used according to the manufacturer's instructions. Therefore, 150–

200 response units of biotinylated B7-H6-Fc protein were immobilized on a Sensor Chip CAP (GE Healthcare). Different analyte concentrations of the NKp30-Fc mutants were sequentially injected over the flow cells at 25 °C with a flow rate of 30 μl/min in the single cycle kinetics model. Data were analyzed using Biacore T200 Evaluation Software version 2.0 (GE Healthcare), and K_D values for the initial NKp30/B7-H6 interaction were determined by bivalent analyte fit. All experiments were carried out at least three times.

Signaling Reporter Assays—A5-GFP cells were either mixed with Ba/F3 Mock or Ba/F3 B7-H6 cells at different effector: target ratios (2:1, 1:1, and 0.5:1) or seeded in 96-well plates coated with NKp30- or NKp46-specific antibodies. A5-GFP cells incubated with 50 ng/ml PMA and 750 ng/ml ionomycin served as the positive control. After overnight incubation at 37 °C, cells were stained with a CD4-specific antibody to distinguish reporter and target cells. For live/dead discrimination, cells were stained with SytoxBlue before measurement. GFP expression of the reporter cells was determined by flow cytometry after gating on $CD4^+$/$SytoxBlue^-$/GFP^+ cells, and data were analyzed using FlowJo software. Statistical significance of flow cytometry experiments was assessed by one-way ANOVA and Dunnett's multiple comparisons test with Prism 6 software to compare GFP expression of the mutants to wild type GFP expression. A probability level of 5% ($p \leq 0.05$) was considered as significant.

Western Blotting Analysis—For Western blotting analysis, cells were detached and resuspended in membrane buffer (10 mM Tris-HCl, pH 7.4, with 50 mM NaCl, 5 mM $MgCl_2$, 320 mM sucrose, and 10 mM NaF) containing protease inhibitor. The cell suspension was sonicated and centrifuged to separate crude membranes from cytosolic proteins. The membrane pellet was resuspended in SDS sample buffer, incubated at 37 °C for 30 min, and centrifuged. The supernatant was applied to SDS-PAGE, and solubilized membrane proteins were detected using NKp30- or NKp46-specific antibodies.

Author Contributions—S. M., S. W., S. B., T. Z., E. P., and J. H. performed the experiments. J. K. designed the study. S. M., S. W., T. Z., J. H., and J. K. analyzed the data. S. M., S. W., S. B., T. Z., E. P., J. H., A. S., and J. K. participated in the discussion and wrote the manuscript. All authors read and approved the final manuscript.

Acknowledgments—We thank Prof. Dr. Andreas Diefenbach for providing non-transduced A5-GFP cells and Prof. Dr. Carsten Watzl for providing Ba/F3 B7-H6 and Mock cells.

References

1. Imai, K., Matsuyama, S., Miyake, S., Suga, K., and Nakachi, K. (2000) Natural cytotoxic activity of peripheral-blood lymphocytes and cancer incidence: an 11-year follow-up study of a general population. *Lancet* **356,** 1795–1799
2. Koch, J., Steinle, A., Watzl, C., and Mandelboim, O. (2013) Activating natural cytotoxicity receptors of natural killer cells in cancer and infection. *Trends Immunol.* **34,** 182–191
3. Lanier, L. L. (2005) NK cell recognition. *Annu. Rev. Immunol.* **23,** 225–274
4. Vivier, E., Tomasello, E., Baratin, M., Walzer, T., and Ugolini, S. (2008) Functions of natural killer cells. *Nat. Immunol.* **9,** 503–510
5. Vivier, E., Ugolini, S., Blaise, D., Chabannon, C., and Brossay, L. (2012) Targeting natural killer cells and natural killer T cells in cancer. *Nat. Rev. Immunol.* **12,** 239–252
6. Farag, S. S., and Caligiuri, M. A. (2006) Human natural killer cell development and biology. *Blood Rev.* **20,** 123–137
7. Moretta, L., Bottino, C., Pende, D., Castriconi, R., Mingari, M. C., and Moretta, A. (2006) Surface NK receptors and their ligands on tumor cells. *Semin. Immunol.* **18,** 151–158
8. Bauer, S., Groh, V., Wu, J., Steinle, A., Phillips, J. H., Lanier, L. L., and Spies, T. (1999) Activation of NK cells and T cells by NKG2D, a receptor for stress-inducible MICA. *Science* **285,** 727–729
9. Pende, D., Parolini, S., Pessino, A., Sivori, S., Augugliaro, R., Morelli, L., Marcenaro, E., Accame, L., Malaspina, A., Biassoni, R., Bottino, C., Moretta, L., and Moretta, A. (1999) Identification and molecular characterization of NKp30, a novel triggering receptor involved in natural cytotoxicity mediated by human natural killer cells. *J. Exp. Med.* **190,** 1505–1516
10. Cantoni, C., Bottino, C., Vitale, M., Pessino, A., Augugliaro, R., Malaspina, A., Parolini, S., Moretta, L., Moretta, A., and Biassoni, R. (1999) NKp44, a triggering receptor involved in tumor cell lysis by activated human natural killer cells, is a novel member of the immunoglobulin superfamily. *J. Exp. Med.* **189,** 787–796
11. Vitale, M., Bottino, C., Sivori, S., Sanseverino, L., Castriconi, R., Marcenaro, E., Augugliaro, R., Moretta, L., and Moretta, A. (1998) NKp44, a novel triggering surface molecule specifically expressed by activated natural killer cells, is involved in non-major histocompatibility complex-restricted tumor cell lysis. *J. Exp. Med.* **187,** 2065–2072
12. Pessino, A., Sivori, S., Bottino, C., Malaspina, A., Morelli, L., Moretta, L., Biassoni, R., and Moretta, A. (1998) Molecular cloning of NKp46: a novel member of the immunoglobulin superfamily involved in triggering of natural cytotoxicity. *J. Exp. Med.* **188,** 953–960
13. Sivori, S., Vitale, M., Morelli, L., Sanseverino, L., Augugliaro, R., Bottino, C., Moretta, L., and Moretta, A. (1997) p46, a novel natural killer cell-specific surface molecule that mediates cell activation. *J. Exp. Med.* **186,** 1129–1136
14. Brandt, C. S., Baratin, M., Yi, E. C., Kennedy, J., Gao, Z., Fox, B., Haldeman, B., Ostrander, C. D., Kaifu, T., Chabannon, C., Moretta, A., West, R., Xu, W., Vivier, E., and Levin, S. D. (2009) The B7 family member B7-H6 is a tumor cell ligand for the activating natural killer cell receptor NKp30 in humans. *J. Exp. Med.* **206,** 1495–1503
15. Binici, J., and Koch, J. (2014) BAG-6, a jack of all trades in health and disease. *Cell. Mol. Life Sci.* **71,** 1829–1837
16. Pogge von Strandmann, E., Simhadri, V. R., von Tresckow, B., Sasse, S., Reiners, K. S., Hansen, H. P., Rothe, A., Böll, B., Simhadri, V. L., Borchmann, P., McKinnon, P. J., Hallek, M., and Engert, A. (2007) Human leukocyte antigen-B-associated transcript 3 is released from tumor cells and engages the NKp30 receptor on natural killer cells. *Immunity* **27,** 965–974
17. Wang, W., Guo, H., Geng, J., Zheng, X., Wei, H., Sun, R., and Tian, Z. (2014) Tumor-released Galectin-3, a soluble inhibitory ligand of human NKp30, plays an important role in tumor escape from NK cell attack. *J. Biol. Chem.* **289,** 33311–33319
18. Rosental, B., Brusilovsky, M., Hadad, U., Oz, D., Appel, M. Y., Afergan, F., Yossef, R., Rosenberg, L. A., Aharoni, A., Cerwenka, A., Campbell, K. S., Braiman, A., and Porgador, A. (2011) Proliferating cell nuclear antigen is a novel inhibitory ligand for the natural cytotoxicity receptor NKp44. *J. Immunol.* **187,** 5693–5702
19. Baychelier, F., Sennepin, A., Ermonval, M., Dorgham, K., Debré, P., and Vieillard, V. (2013) Identification of a cellular ligand for the natural cytotoxicity receptor NKp44. *Blood* **122,** 2935–2942
20. Tomasello, E., Desmoulins, P. O., Chemin, K., Guia, S., Cremer, H., Ortaldo, J., Love, P., Kaiserlian, D., and Vivier, E. (2000) Combined natural killer cell and dendritic cell functional deficiency in KARAP/DAP12 loss-of-function mutant mice. *Immunity* **13,** 355–364
21. Hall, C., Berkhout, B., Alarcon, B., Sancho, J., Wileman, T., and Terhorst, C. (1991) Requirements for cell surface expression of the human TCR/CD3 complex in non-T cells. *Int. Immunol.* **3,** 359–368

22. Kappes, D. J., and Tonegawa, S. (1991) Surface expression of alternative forms of the TCR/CD3 complex. *Proc. Natl. Acad. Sci. U.S.A.* **88,** 10619–10623
23. Sussman, J. J., Bonifacino, J. S., Lippincott-Schwartz, J., Weissman, A. M., Saito, T., Klausner, R. D., and Ashwell, J. D. (1988) Failure to synthesize the T cell CD3-ζ chain: structure and function of a partial T cell receptor complex. *Cell* **52,** 85–95
24. Call, M. E., Schnell, J. R., Xu, C., Lutz, R. A., Chou, J. J., and Wucherpfennig, K. W. (2006) The structure of the $\zeta\zeta$ transmembrane dimer reveals features essential for its assembly with the T cell receptor. *Cell* **127,** 355–368
25. Arnaud, J., Chenu, C., Huchenq, A., Gouaillard, C., Kuhlmann, J., and Rubin, B. (1996) Defective interactions between TCR chains and CD3 heterodimers prevent membrane expression of TCR-$\alpha\beta$ in human T cells. *J. Immunol.* **156,** 2155–2162
26. Binici, J., Hartmann, J., Herrmann, J., Schreiber, C., Beyer, S., Güler, G., Vogel, V., Tumulka, F., Abele, R., Mäntele, W., and Koch, J. (2013) A soluble fragment of the tumor antigen BCL2-associated athanogene 6 (BAG-6) is essential and sufficient for inhibition of NKp30 receptor-dependent cytotoxicity of natural killer cells. *J. Biol. Chem.* **288,** 34295–34303
27. Hartmann, J., Tran, T. V., Kaudeer, J., Oberle, K., Herrmann, J., Quagliano, I., Abel, T., Cohnen, A., Gatterdam, V., Jacobs, A., Wollscheid, B., Tampé, R., Watzl, C., Diefenbach, A., and Koch, J. (2012) The stalk domain and the glycosylation status of the activating natural killer cell receptor NKp30 are important for ligand binding. *J. Biol. Chem.* **287,** 31527–31539
28. Herrmann, J., Berberich, H., Hartmann, J., Beyer, S., Davies, K., and Koch, J. (2014) Homo-oligomerization of the activating natural killer cell receptor NKp30 ectodomain increases its binding affinity for cellular ligands. *J. Biol. Chem.* **289,** 765–777
29. Cheung, J. C., and Reithmeier, R. A. (2005) Membrane integration and topology of the first transmembrane segment in normal and Southeast Asian ovalocytosis human erythrocyte anion exchanger 1. *Mol. Membr. Biol.* **22,** 203–214
30. Hofmann, K., and Stoffel, W. (1993) TMBASE-a database of membrane spanning protein segments. *Biol. Chem. Hoppe-Seyler* **374,** 166
31. Nilsson, I. M., and von Heijne, G. (1993) Determination of the distance between the oligosaccharyltransferase active site and the endoplasmic reticulum membrane. *J. Biol. Chem.* **268,** 5798–5801
32. Popov, M., Li, J., and Reithmeier, R. A. (1999) Transmembrane folding of the human erythrocyte anion exchanger (AE1, Band 3) determined by scanning and insertional *N*-glycosylation mutagenesis. *Biochem. J.* **339,** 269–279
33. Popov, M., Tam, L. Y., Li, J., and Reithmeier, R. A. (1997) Mapping the ends of transmembrane segments in a polytopic membrane protein: scanning *N*-glycosylation mutagenesis of extracytosolic loops in the anion exchanger, band 3. *J. Biol. Chem.* **272,** 18325–18332
34. Cheung, J. C., and Reithmeier, R. A. (2007) Scanning *N*-glycosylation mutagenesis of membrane proteins. *Methods* **41,** 451–459
35. Sun, Z. J., Kim, K. S., Wagner, G., and Reinherz, E. L. (2001) Mechanisms contributing to T cell receptor signaling and assembly revealed by the solution structure of an ectodomain fragment of the CD3 $\epsilon\gamma$ heterodimer. *Cell* **105,** 913–923
36. Joyce, M. G., Tran, P., Zhuravleva, M. A., Jaw, J., Colonna, M., and Sun, P. D. (2011) Crystal structure of human natural cytotoxicity receptor NKp30 and identification of its ligand binding site. *Proc. Natl. Acad. Sci. U.S.A.* **108,** 6223–6228
37. Li, Y., Wang, Q., and Mariuzza, R. A. (2011) Structure of the human activating natural cytotoxicity receptor NKp30 bound to its tumor cell ligand B7-H6. *J. Exp. Med.* **208,** 703–714
38. Smith-Garvin, J. E., Koretzky, G. A., and Jordan, M. S. (2009) T cell activation. *Annu. Rev. Immunol.* **27,** 591–619
39. Bolliger, L., Johansson, B., and Palmer, E. (1997) The short extracellular domain of the T cell receptor ζ chain is involved in assembly and signal transduction. *Mol. Immunol.* **34,** 819–827
40. John, S., Banting, G. S., Goodfellow, P. N., and Owen, M. J. (1989) Surface expression of the T cell receptor complex requires charged residues within the α chain transmembrane region. *Eur. J. Immunol.* **19,** 335–339
41. Aivazian, D., and Stern, L. J. (2000) Phosphorylation of T cell receptor ζ is regulated by a lipid dependent folding transition. *Nat. Struct. Biol.* **7,** 1023–1026